

Simulation environment of X-ray rotational angiography using 3D+t coronary tree model

Guanyu Yang, Yining Hu, Xi Huang, Huazhong Shu, Christine Toumoulin

▶ **To cite this version:**

Guanyu Yang, Yining Hu, Xi Huang, Huazhong Shu, Christine Toumoulin. Simulation environment of X-ray rotational angiography using 3D+t coronary tree model. EMBC 2012, Aug 2012, United States. pp.629 - 632, 10.1109/EMBC.2012.6346010 . inserm-00770479

HAL Id: inserm-00770479

https://inserm.hal.science/inserm-00770479

Submitted on 6 Jan 2013

HAL is a multi-disciplinary open access archive for the deposit and dissemination of scientific research documents, whether they are published or not. The documents may come from teaching and research institutions in France or abroad, or from public or private research centers.

L'archive ouverte pluridisciplinaire **HAL**, est destinée au dépôt et à la diffusion de documents scientifiques de niveau recherche, publiés ou non, émanant des établissements d'enseignement et de recherche français ou étrangers, des laboratoires publics ou privés.

Simulation Environment of X-Ray Rotational Angiography Using 3D+*t* Coronary Tree Model

Guanyu YANG[1,3], Yining HU[1,3], Xi HUANG[1,3], Huazhong SHU[1,3], Christine Toumoulin[2,3]

***Abstract*—The newly introduced cardiac rotational angiography (RA) can provide a large amount of projections from different angles which greatly improve the 3D coronary tree reconstruction. However, the reconstruction methods are difficult to be objectively evaluated due to the complicated topology of coronary tree and non-linear cardiac motion. In this paper, we present a simulation environment of rotational angiography acquisition system to facilitate the improvements and the evaluations of reconstruction algorithms. A 3D+*t* coronary tree model reconstructed from MSCT sequence is employed to enhance the reality of simulation. A simulation environment of X-ray coronary angiography is developed based on distance-driven projection algorithm. The static angiography is firstly simulated to verify the dynamic model by comparing the displacements of landmarks with the real static angiography of the same patient. Rotational simulation results are then obtained with real system parameters to provide a complete and true-to-life RA sequence representing the morphology of moving coronary tree.**

***Index Terms*—Coronary Artery, Rotational Angiography, Simulation, 3D+*t* model.**

I. Introduction

Today, over 1 million Percutaneous transluminal coronary angioplasty (PTCA) interventions are performed each year worldwide for the treatment of angina and myocardial infarction. Cardiologists, who are today under tremendous time constraint, ask for new advances in angiography imaging techniques to improve both the safety and the efficacy of coronary angiography or interventions. Recently, a new image acquisition has been introduced, in the form of rotational angiography (RA) that allows cardiologists to obtain up to 180 projections of the left or right coronary tree during a single injection of contrast under different angles (caudal, cranial, axial). It provides thus a complete range of projections, giving a pseudo 3D view of the coronary tree. The marriage of rotational angiography with rapid, online 3D coronary reconstruction or modeling would allow improving the accuracy of the measurement for the lesion assessment, choosing the adequate material (catheter size, type of stents, etc.) and guiding the catheter while negotiating the trajectory in the tortuous vascular segments, up to the site to be treated and precisely place the balloon or the stent. Over the last decade, 3D coronary reconstruction algorithms has been addressed first through computer vision approaches using mono- and biplane systems with epipolar techniques and feature matching in order to find corresponding primitives and retrieve their 3D geometry. However, the resolution of this ill-posed problem requires either a prior model[1], additional views[2] or the joint use of motion [3]. Recently the full 3D reconstruction from a single rotational projection sequence takes benefit from the higher number of projections (more than 50) by using tomographic methods[4][5]. Nevertheless the quality and the accuracy of reconstruction need to be objectively evaluated. Different solutions can be considered such as the animal experimentation or the acquisition system modeling with the 3D physical or numerical phantom building. This paper describes a simulation environment by using a 3D+*t* model to evaluate the 3D reconstruction algorithm of the coronary arteries. It includes three parts: (1) The construction of a patient-specific 3D+*t* model of the coronary tree from dynamic volume sequence of multi-slice computed tomography (MSCT). The result is a sequence of volumes representing the motion of the coronary arteries throughout the cardiac cycle (section II); (2) The modeling of the rotational angiography acquisition system to simulate different acquisition and gating strategies (section III); (3) The calculation of radiographic projections of the 3D model of coronary tree (section IV). Section V provides some preliminary results and discussion with a comparison with real data. Section VI concludes on the results.

II. 3D+*t* Coronary Artery Model Construction

MSCT as a non-invasive imaging modality can obtain ten volumes at every 10% phase of cardiac cycle between R-R peaks by using ECG-gating technique. The consecutive volume sequence carrying cardiac motion advances 3D+*t* heart model reconstruction including cardiac cavities and coronary artery tree. We present a methodology for coronary tree model construction which is summarized in Fig. 1. The reconstruction procedure contains three steps:(1) Centerline extraction of coronary arteries in each volume of MSCT sequence; (2) Point-based matching to estimate cardiac motion parameters; (3) 4D model generation based on estimated motion parameters. A dynamic model is generated by deforming an end-diastolic model by estimated motion parameters.

Primitive centerlines of coronary arteries were extracted by our tracing-based method in every MSCT volume [6]. Starting from the user-defined seed points, the centerline points can be iteratively searched with estimating local diameter simultaneously. A constrained point-based matching method was then developed to represent the cardiac motion by B-

[1] Laboratory of Image Science and Technology, School of Computer Science and Engineering, Southeast University, 210096, Nanjing, China
[2] INSERM UMR 1099, Laboratoire de Traitement du Signal et d'Image, Université de Rennes 1, 35042, Rennes, France
[3] Centre de Recherche en Information Biomédicale sino-français (CRIBs)
* Correspondence information: Guanyu Yang, yang.list@seu.edu.cn

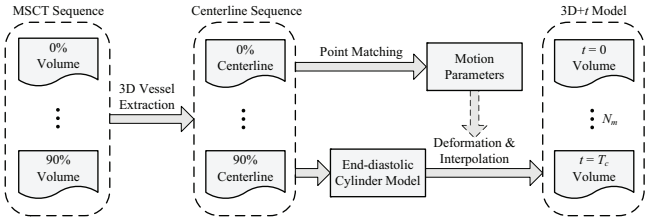


Fig. 1. Flowchart of 3D+*t* coronary tree model reconstruction.

spline basis functions [7]. Feature points such as bifurcations and coronary ostia serve as constraints by keeping their correspondence to maintain the coronary topology during point matching. By minimizing an energy function, the optimal transformation function ϕ_t and the optimal correspondence W_t can be acquired for each two consecutive cardiac phases t and $t+1$. The extracted end-diastolic centerlines from MSCT data set are then consecutively deformed by ϕ_t to estimate motion vectors of centerline points at each phase t. The centerlines of middle states between phase t and $t+1$ are approximated by motion vectors. With estimated local diameters, N_m volumes representing the temporal morphologies of coronary during a whole cardiac cycle T_c can be finally generated.

III. Rotational Angiography System Modeling

The RA system is composed of an X-ray source and an image intensifier mounted on a motorized computer controlled arc known as the C-arm. The X-ray source is fixed with respect to the center of rotation or the origin of system coordinates (Center *C*). The source - intensifier plane distance (*SID*) and the source - Center *C* distance (*SCD*) specify the size of C-arm and rotation radius. The entire assembly can rotate along an arc around a table, allowing multiple acquisitions from different angles (Fig. 2). Two angles, named primary angle θ and secondary angle φ respectively, control the orientation of the C-arm. φ is kept constant over the acquisition time and can be set to an arbitrary value between $-30°$ cranial (CRA) to $30°$ caudal (CAU). θ refers to rotation angle normally ranging from a specified right anterior oblique (RAO) angle to a left anterior oblique (LAO) angle with angular increment θ_{step} ($1.5°$–$5°$) applied during the C-arm rotation. And frame time T_f determines the temporal resolution of the sequence.

The 3D+*t* coronary tree model, represented by a series of volumes during one cardiac cycle, is placed at center *C* by translating the user-defined rotation center coinciding with *C*. During the simulation, the volume will be automatically loaded based on the time, the size of isotropic volume and its spatial resolution, $N_x^V \times N_y^V \times N_z^V$ and S^V, are specified by MSCT data. Whereas, the size of projection image and its spatial resolution, $N_x^I \times N_y^I$ and S^I, can be defined according to different simulation strategies.

IV. Projection Calculation

Radiographic projection can be directly calculated by ray-tracing based algorithms such as digitally reconstructed radiographs (DRRs)[8]. Nevertheless, the high computation complexity of ray-tracing based algorithms limited their application to RA simulation of more than 80 high resolution projections.

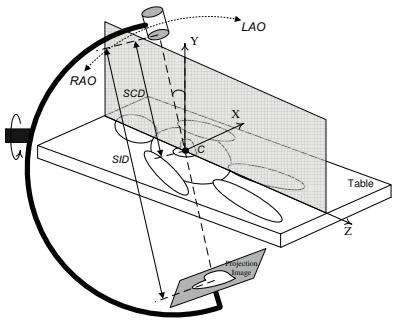


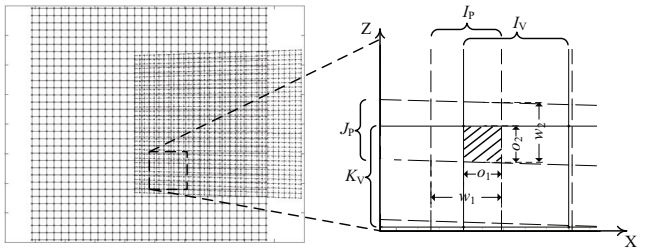
Fig. 2. Geometry of 3D-RA system.

The distance-driven projection algorithm [9] is adopted to perform the projection simulation owing to its good computation performance. The algorithm relies on a bijective mapping that each voxel within a specified image slice of 3D volume data can uniquely be mapped on a single point on 2D intensifier plane. At each angle, the boundaries of voxel and pixel can be mapped to a common plane to generate overlap region. The area of overlap region of mapped voxel and mapped pixel can then serve as the coefficient for the line integrals. The manipulation of coordinates mapping accelerates the computation by avoiding the loop over all the dimensions of the volume data and projection image.

The calculation starts with coordinates mapping. At each angle θ, the boundaries of voxels within every image slice of volume data and pixels within the intensifier plane need to be mapped on a specified plane P. The plane parallel to the image slice in the volume such as XZ plane ($Y = 0$) or YZ plane ($X = 0$) in our system is chosen for coordinates mapping to ensure the coordinates of slices map to a uniform grid maintaining the original shape. A coordinates mapping example on XZ plane with θ = RAO30° and $\varphi = 0°$ is illustrated in Fig. 3(a). The squared grid and the trapezoid grid represent the mapped boundaries of voxel in image slice and pixel in intensifier plane respectively. A magnification shows the overlap detail of the voxel V and the pixel P in Fig. 3(b) by marking the overlap region with diagonals. In order to simplify the computation, the overlap area can be approximated by the area of the rectangle with lengths of sides equal to o_1 and o_2. The mapped pixel area can be estimated similarly by w_1 and w_2. The ratio of these two areas is finally used as the coefficient to calculate the contribution of voxel V to the pixel P, which is defined by

$$l^V = \frac{s}{\cos\alpha\cos\gamma}\frac{o_1 o_2}{w_1 w_2}\mu_V \tag{1}$$

where s refers to the isotropic voxel size, α and γ defines the in-plane angles of the projections of the ray traveling from source to pixel P with the axes Y in XY and YZ plane respectively. $(s/\cos\alpha\cos\gamma)$ gives the length of intersected



(a) (b)

Fig. 3. (a) Coordinates mapping with θ = RAO30°, φ = 0°. Mapped grids of volume slice and intensifier plane are represented by solid and dashed lines respectively. (b) overlap area calculation. The overlap region of voxel $V(I_V, J_V, K_V)$ and pixel $P(I_P, J_P)$ in (a) is magnified and marked with diagonals.

ray in V. And μ_V is linear attenuation coefficient of V which can be acquired by the attenuation coefficient of water [8]. By accumulating all the voxel contributions to pixel P, the receiving energy of P is defined as

$$I_P = I_0 e^{-\sum_{i=1}^{M} l_i^V} \tag{2}$$

where I_0 is the incident x-ray energy, and M is the number of voxels who have contributions to P.

During the cardiac angiography, contrast agent is injected into coronary tree to distinguish them with other structures. The background of real angiography needs to be simulated to enhance the reality of simulation. Besides a series of binary volumes marking the region of interested coronary tree, a raw volume reconstructed from MSCT data is employed to generate the background of angiography. Parameters a_i is adopted to enhance the l_i^V of the voxels inside the interested region and decrease the l_i^V of the voxels outside the interested region. Eq. 2 can be rewritten as

$$I_P = I_0 e^{-\left(\sum_{i=1}^{M} a_i l_i^V\right)} \tag{3}$$

where a_i is specified to 2.0 and 0.2 for the voxels inside and outside the vessel region respectively.

V. Results and Discussion

A. 3D+t Model

Five MSCT sequences were used to reconstruct patient-specific coronary tree model. Breath-hold volume sequences were imaged by Siemens 64-slices CT with about 0.3 mm^2 pixel size and 0.75mm slice thickness. The size of axial images is 512×512. The isotropic volumes were obtained after interpolation. As motion artifacts inevitably exist in current MSCT sequence during early systole period, additional user interaction and physician evaluation are necessary to ensure the accuracy of centerlines before labeling all the branches with their anatomical names. One of the final 3D+*t* coronary tree model generated from these datasets is illustrated in Fig. 4. The model is limited to the left coronary artery (LCA) including left anterior descending (LAD), left circumflex (LCx) and their sub-branches. The morphologies

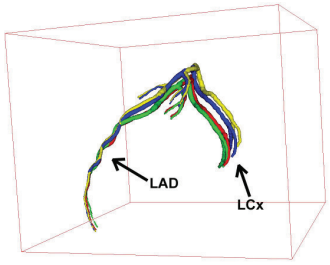


Fig. 4. 3D+*t* coronary tree model. The vessel morphology of four main phases along a cardiac cycle are displayed with different colors: mid-systole(■), end-systole(■), mid-diastole(■) and end-diastole(■).

at four principal cardiac phases, i.e. mid-(■), end-systole(■) and mid-(■), end-diastole(■), are demonstrated together to show the cardiac motion.

B. Projection Results

1) Static Simulation Results: Before performing RA simulation, we firstly simulated a static angiography in order to verify the projections and the 3D+*t* model by comparing with a real static angiography sequence of the same patient. We adopted the same acquisition parameters of the real data with SID = 1038mm, SCD = 765mm, θ = LAO2.4°, φ = −25.9°, $N_x^I = N_y^I$ = 512, S^I = 0.258mm and $T_f = 1/15$s. The volume of the model was translated to ensure the coronary tree to be centered in the projection images. The heart rate (HR) of model was estimated by the real data, HR = 69bpm. Thus, 14 projections were simulated during a cardiac cycle with the first projection corresponding to the beginning of systole period. In Fig. 5, two projections are shown by comparing with the corresponding frames in the real sequence. The real frames are carefully chosen from the stasis period of respiration in order to avoid unexpected respiration motion. The simulated projections have the similar morphology of coronary tree and intensity distribution to the real projections.

Two landmarks, i.e. LAD-LCx bifurcation and obtuse marginal(OM)-LCx bifurcation, are selected to verify the model by tracing their movements in the simulated and the real projections respectively. Fig. 6 presents the 2D in-plane displacement curves of two landmarks. The curves of simulated projections have the alike shape with the ones of real projection with the maximum displacements locating near the $0.4T_c$ which corresponds to the instant of end-systole. Statistical research on displacements in [10] concluded the similar results of cardiac motion. The small difference between the curves may ascribe to the orientation difference of patient, respiration motion in the real data and inaccurate heart rate estimation.

2) Rotational Simulated Projections: 3D-RA simulation was then performed by setting the acquisition parameters as SID = 1103mm, SCD = 690mm, θ = RAO29°-LAO90°, θ_{step} = 1.5°, φ = 0°, $N_x^I = N_y^I$ = 512, S^I = 0.278mm and $T_f = 1/30$s. The simulated sequence of 79 projections was obtained and 10 of them were displayed in Fig. 7

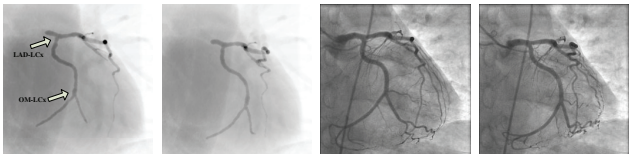


Fig. 5. Static sequence comparison between simulated projections (left two figures) and real projections (right two figures), representing the states of end-diastole and end-systole of simulated and real projections respectively. LAD-LCx and OM-LCx bifurcations are noted.

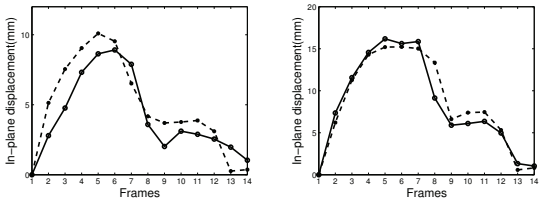


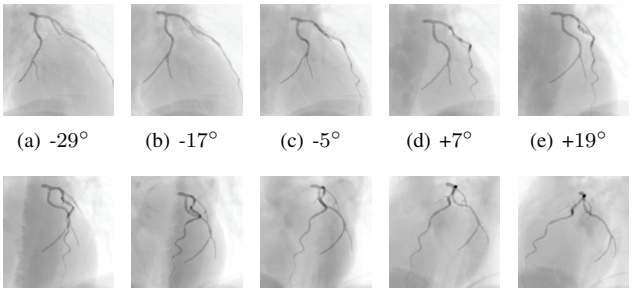
Fig. 6. The in-plane displacement comparison between real data (solid line) and simulated data (dashed line) for LAD-LCx (left) and OM-LCx bifurcation (right) marked in Fig. 5.

with 12° intervals. As the HR was set to 69bmp, the projections were obtained within 3 cardiac cycles, which can be observed by the change of in-plane vertical displacement. The whole sequence can be calculated within 30mins by a common computer (Intel Core2 Duo T5500, 2G RAM). The computation time can be improved by parallel computation technique with GPU.

The simulated RA sequence can represent the skeleton of coronary tree from different angle with real cardiac motion. However, some differences inevitably exist between the simulated and the real angiography. Firstly, some sub-branches of coronary tree can not be extracted from MSCT data because of motion artifacts. Only main coronary arteries are included in the current model, which greatly limits the reality of simulation. Secondly, the manner of agent contrast using also enlarges their differences. In the MSCT the blood with contrast agent flowed all over the body, while, in RA the contrast agent congregated in the interested branches during the imaging. As a result, the background of RA typically composed of vertebral column, costal bones and lung was blurred with cardiac cavities, aorta and pulmonary arteries in the simulated projections. Furthermore, MSCT only focuses the imaging region around heart. By using the raw volume without some anatomical structures such as ribs, spinal column and lungs, it is difficult to generate the same background as the real angiography.

VI. Conclusion

In this paper, we present a simulation environment of RA acquisition system to facilitate the improvements and the evaluations of reconstruction algorithms based on RA. The 3D+*t* coronary tree model is firstly generated based on MSCT sequence in order to enhance the reality of simulation. Distance-driven algorithm can efficiently calculate radiographic projections. The static angiography is firstly simulated to verify the projections and the dynamic model by comparing it with the real static angiography of the same patient. Rotational simulation results of high-resolution projections are then obtained with real system parameters to provide a complete and true-to-life RA sequence representing the morphology of moving coronary tree. This environment has been used in the preliminary studies of RA reconstruction algorithm [11].



(a) -29° (b) -17° (c) -5° (d) +7° (e) +19°

(f) +31° (g) +43° (h) +55° (i) +67° (j) +79°

Fig. 7. RA simulation sequence with θ from $\mathrm{RAO}(-)29^\circ$ to $\mathrm{LAO}(+)90^\circ$, $\varphi = 0^\circ$. The illustrated images from (a) to (j) are selected out with each 12° interval.

Acknowledgment

Supported by National Natural Science Foundation of China (No. 81101104 and No. 31100713).

References

[1] M. Garreau,J. L. Coatrieux, R. Collorec, C. Chardenon, "A knowldege-based approach for 3D re-construction and labeling of vascular network from biplance angiographic projections," IEEE Trans. Med. Imag., vol. 10, pp. 122–131, 1991.

[2] C. Venaille, D. Mishler, J. L. Coatrieux, "Un algorithme peu contraint d'appariement de primitives courbes par stereovision trnoculaire," Rev. Technique Thomson CSF, vol. 24, pp.1071–1099, 1992.

[3] S. Ruan, A. Bruno, J. L. Coatrieux, "Three dimensional motion and reconstruction of coronary arteries from biplane cineangiography," Image Vis. Comput., vol. 12, pp.683–689, 1994.

[4] C. Blondel, G. Malandiain, R. Vaillant, N. Ayache, "Reconstruction of Coronary Arteries From a Single Rotational X-Ray Projection Sequence," IEEE Trans. Med. Imag., vol.25, pp.653–663, 2006

[5] J. Zhou, A. Bousse, G. Yang, J. J. Bellanger, L. Luo, C. Toumoulin, J. L, Coatrieux, "A Blob-Based Tomographic Reconstruction of 3D Coronary Trees from Rotational X-ray Angiography," SPIE Med. Imag., San Diego, USA, pp.16–21, 2008.

[6] G. Yang, A. Bousse, C. Toumoulin, H. Shu, "A Multiscale Tracking Algorithm for the Coronary Extraction in MSCT Angiography," 28th Annual Conference of the IEEE Engineering in Medicine and Biology Society (EMBS), pp.3066–3069, 2006.

[7] G. Yang, J. Zhou, D. Boulmier, M-P. Garcia, L. Luo, C. Toumoulin, "Characterization of 3-D Coronary Tree Motion from MSCT Angiography", IEEE Trans. Inf. Technol. Biomed., vol.14, no.1, pp.101–106, 2010.

[8] N. Milickovic, D. Baltas, S. Giannouli, M. Lahanas, N. Zamboglou, "CT imaging based digitally reconstructed radiographs and their application in brachytherapy," Phys. Med. Biol., vol.45, pp.2787-2800, 2000.

[9] B. De Man, S. Basu, "Distance-driven projection and backprojection in three demensions," Phys. Med. Biol., vol.49, pp.2463–2475, 2004.

[10] G. Shechter, J. Resar, E. McVeigh, "Displacement and Velocity of the Coronary Arteries: Cardiac and Respiratory Motion," IEEE Trans. Med. Imag., vol.25, pp.369-375, 2006.

[11] Y. Hu, L. Xie, J.C. Nunes, J. J. Bellanger, M. Bedossa, C. Toumoulin, "ECG gated tomographic reconstruction for 3-D rotational coronary angiography," 34th Annual Conference of the IEEE Engineering in Medicine and Biology Society (EMBS), pp. 3614–3617, 2010.